TISSUE ENGINEERING: Part A
Volume 20, Numbers 3 and 4, 2014

DOI: 10.1089/ten.tea.2013.0170

Human Endometrial Mesenchymal Stem Cells Modulate the Tissue Response and Mechanical Behavior of Polyamide Mesh Implants for Pelvic Organ Prolapse Repair

Daniela Ulrich, MD,[1,2,*] Sharon Lee Edwards, PhD,[3] Kai Su, PhD,[3] Ker Sin Tan, MSc,[1] Jacinta F. White, BApplSci,[3] John A.M. Ramshaw, PhD,[3] Camden Lo, PhD,[1] Anna Rosamilia, MD, PhD,[2] Jerome A. Werkmeister, PhD,[3,†] and Caroline E. Gargett, PhD[1,2,†]

Background: Pelvic organ prolapse (POP) is defined as the descent of one or more of the pelvic structures into the vagina and includes uterine, vaginal vault, and anterior or posterior vaginal wall prolapse. The treatment of POP may include implantation of a synthetic mesh. However, the long-term benefit of mesh surgery is controversial due to complications such as mesh exposure or pain. The aim of this study was to use a tissue engineering (TE) approach to assess the *in vivo* biological and biomechanical behavior of a new gelatin/polyamide mesh, seeded with a novel source of mesenchymal stem cells in a subcutaneous rat model of wound repair.
Methods: W5C5-enriched human endometrial mesenchymal stem cells (eMSC) were seeded onto meshes (gelatin-coated polyamide knit) at 100,000 cells/cm^2. Meshes, with or without cells were subcutaneously implanted dorsally in immunocompromised rats for 7, 30, 60, and 90 days. Flow cytometry was used to detect DiO labeled cells after explantation. Immunohistochemical assessment of foreign body reaction and tissue integration were conducted. Total collagen and the levels of collagens type III and type I were determined. Uniaxial tensiometry was performed on explanted meshes, originally seeded with and without cells, at days 7 and 90.
Results: Implanted meshes were well tolerated, with labeled cells detected on the mesh up to 14 days postimplantation. Meshes with cells promoted significantly more neovascularization at 7 days ($p < 0.05$) and attracted fewer macrophages at 90 days ($p < 0.05$). Similarly, leukocyte infiltration was significantly lower in the cell-seeded meshes at 90 days ($p < 0.05$). Meshes with cells were generally less stiff than those without cells, after 7 and 90 days implantation.
Conclusion: The TE approach used in this study significantly reduced the number of inflammatory cells around the implanted mesh and promoted neovascularization. Seeding with eMSC exerts an anti-inflammatory effect and promotes wound repair with new tissue growth and minimal fibrosis, and produces mesh with greater extensibility. Cell seeding onto polyamide/gelatin mesh improves mesh biocompatibility and may be an alternative option for future treatment of POP.

Introduction

Pelvic organ prolapse (POP) is defined as the descent of one or more of the anterior or posterior vaginal wall, the uterus, or the apex of the vagina after hysterectomy.[1] POP commonly occurs several years after childbirth, but aging and obesity also contribute to the pathophysiology.[2] Almost one in four women in the United States suffers from one or more symptoms of POP, with urinary incontinence the most common.[3] Other symptoms include sexual dysfunction, discomfort due to tissue protrusion, back pain, and voiding or defecatory difficulty. Symptoms range in severity and depend, in part, on the degree and type of prolapse. While less severe stages of POP can be managed conservatively, more severe stages, or symptoms affecting the patient's quality of life, often require surgical repair. Due to reports of the high objective failure rate of native tissue surgery reconstruction (up to 35% in the long term), synthetic meshes were introduced to augment POP surgery, with better anatomical success rates in the long term.[4,5] Polypropylene (PP) meshes are the most commonly used meshes and are knitted from monofilaments to produce a relatively large pore size for allowing tissue ingrowth.[6] These current therapies provide support but do not replace lost or damaged tissues of

[1]The Ritchie Centre, Monash Institute of Medical Research, Clayton, Victoria, Australia.
[2]Department of Obstetrics and Gynaecology, Monash Medical Centre, Monash University, Clayton, Victoria, Australia.
[3]Materials Science Engineering, CSIRO, Clayton, Victoria, Australia.
*Current affiliation: Department of Obstetrics and Gynaecology, Medical University of Graz, Austria.
†These authors are equal senior authors.

the pelvic support structures including the pelvic floor musculature, endopelvic fascia, and ligaments.[7] A recent FDA report warned of the complications associated with the use of PP mesh for vaginal surgery.[8,9] Implanted meshes initiate an inflammatory reaction involving cells of the innate immune system, which results in the initial production of neotissue. However, the new tissue develops into scar tissue, which is weaker and more rigid than normal healthy tissue.[10,11] This may translate into significant long-term complications of varying severity including mesh contraction, pain, and vaginal exposure or rarely erosion to adjacent viscera; these complications have been reported in up to 29% of cases.[12]

Tissue engineering (TE) approaches have been used in different medical areas to improve long-term outcomes of surgical interventions. Bone marrow mesenchymal stem cells (bmMSC) are believed to regulate the repair process in injured tissue sites by interacting with essential endogenous cells involved in the healing process; fibroblasts, endothelial, and epithelial cells.[13] Mouse muscle-derived stem cells cultured on porcine small intestinal submucosa (SIS) collagen (Cook, Biotech®), and implanted as a TE construct into rat vaginal defects, stimulated vaginal tissue repair by promoting epithelial regeneration and reducing fibrosis.[14] Clinically, SIS has been trialed for POP restoration with very limited success compared with conventional synthetic mesh types.[15] More recently, it was shown that Vicryl® hernia meshes seeded with bmMSC were associated with less adhesions in a rat abdominal hernia model compared with cell-free hernia meshes.[16] This study also found that mesh pore size played a major role in cell attachment and proliferation, with mesh pores larger than 3 mm prohibiting cell attachment.[16] We have identified and characterized human endometrial mesenchymal stem cells (eMSC) as an easily obtainable source of mesenchymal stem cells (MSC) by minimal invasive procedures not requiring an anesthetic.[17,18] In contrast, bmMSC and adipose tissue MSC require procurement methods necessitating local or general anesthesia and significant discomfort. Methods have been developed to isolate the eMSC prospectively using the CD146 and CD140b[19,24] or the W5C5 markers.[20] We have recently shown that it should be possible to prepare suitable quantities of eMSC under good manufacturing practice (GMP) for clinical application.[21] More recently, given the perceived issues with some of the clinical PP meshes, we have also developed new meshes from alternative biomaterials, with some improved mechanical properties[22] and shown that a gelatin-coated polyamide mesh had improved tissue integration in a rat abdominal hernia model, compared with a conventional PP clinical mesh.[23]

The aim of this study was to determine the *in vivo* host tissue response and biomechanical properties of a new gelatin-coated polyamide knitted mesh seeded with eMSC using a rat wound model as a preclinical model for POP repair surgery.

Materials and Methods

Human tissue

Informed written consent was obtained from each patient and ethics approval was obtained from the Southern Health Human Research and Ethics Committee B. Human endometrial tissue was collected from two patients undergoing hysterectomy and isolated cells were obtained as published previously.[20] Briefly, the endometrium was scraped from the myometrium and finely minced, then digested in collagenase I and DNase I in Dulbecco's modified Eagle's medium (DMEM)/F12 culture medium (Life Technologies) in 5% CO_2 in air at 37°C. Following digestion, the cells were filtered through a cell strainer to obtain the stromal fraction followed by Ficoll Paque to remove red blood cells. The eMSC were extracted using magnetic beads and the single marker antibody, W5C5 as described recently.[20] The cells were cultured in DMEM/F12 medium containing 10% fetal calf serum, 1% antibiotic-antimycotic (100 U/mL penicillin, 100 µg/mL streptamycin, 0.25 µg/mL fungizone; Life Technologies), and 2 mM glutamine (culture medium) up to passage 6 (P6) to obtain sufficient cell numbers for implantation into rats.

Properties of cultured W5C5$^+$ adherent cells

As MSC are known to change their properties in culture, analysis of colony-forming unit activity and differentiation assays were performed on P6 cells to determine MSC properties as previously described.[18,21] Briefly, cloning efficiency was determined by seeding the W5C5 bead-sorted cells at clonal densities (50–200 cells/cm^2) on fibronectin (10 µg/mL)-coated 100 mm diameter culture dishes. Cells were incubated at 37°C in 5% CO_2 for at least 2 weeks with weekly media changes. Cloning efficiency was compared with P0 W5C5$^+$ eMSC, as previously published.[20]

To assess multipotency, the P6 cells were cultured in four-well plates in specific adipogenic, chondrogenic, smooth muscle cell, and osteoblast differentiation induction media for 4 weeks as described previously.[18,20] Adipogenic differentiation was evaluated using Oil red O staining to detect lipid droplet accumulation; chondrogenic differentiation by Alcian blue staining; myogenic differentiation by alpha-smooth muscle actin (αSMA) immunostaining; and osteogenic differentiation by alkaline phosphatase histochemistry (Sigma-Aldrich).

Surface marker phenotyping by flow cytometry

Phenotyping of eMSC was done by single-color flow cytometry using known eMSC surface phenotypic markers (W5C5, CD140b, and CD146)[20,24] and more general MSC markers (CD29, CD44, CD73, and CD105)[25] and for negative markers CD34 (hematopoietic marker) and CD45 (myeloid cells) as previously published[20,26] (details of antibodies shown in Table 1). A minimum of 50,000 P6 eMSC were incubated with individual antibodies in separate tubes. Phycoerythrin-labeled secondary antibodies were used to detect labeled cells using a MoFlo® XDP cell sorter (Beckman Coulter). Data were analyzed using Summit Software v5.2. The percentage of positive cells was based on IgG isotype antibodies used for control setting of gates.

Cell labeling

Before implantation, P6 cells were labeled with Vybrant™ DiO reagent (Life Technologies) according to the manufacturer's instructions. Briefly, cells were incubated with 5 µL DiO for 2 min at 37°C and excess dye was then removed by three washes in phosphate-buffered saline (PBS). The labeled cells were detected using a 540/30 bandpass filter.

Preparation of eMSC-seeded mesh constructs

Polyamide meshes were warp knitted and gelatin coated (PA + G) by dip-coating in 12% porcine gelatin, as previously

Table 1. Antibodies Used for Flow Cytometry

Primary antibody	*Clone*	*Concentration (μg/mL)*	*Isotype*	*Supplier*
CD29	mAb13	10	Rat IgG2a	BD Pharmingen
CD31	M89D3	10	Mouse IgG2a	BD Pharmingen
CD44	G44–26	10	Mouse IgG2b	BD Pharmingen
CD45	HI30	10	Mouse IgG1	CALTAG Laboratories
CD73	AD2	10	Mouse IgG1	BD Pharmingen
CD90	5E10	10	Mouse IgG1	BD Pharmingen
CD105	266	10	Mouse IgG1	BD Pharmingen
CD140b (PDGFRβ)	PR7212	25	Mouse IgG1	R&D Systems
CD146	CC9	25	Mouse IgG2a	Donated by P. Simmons, Peter MacCallum Cancer Centre
W5C5	W5C5	25	Mouse IgG1	Donated by Dr. Hans-Jörg Bühring, Tübingen University

described,[23] but in the present study were cross-linked with 0.025% (w/v) glutaraldehyde. PA+G meshes were cut into samples of dimensions 10×25 mm, with the longitudinal axis cut in either the machine (warp) or cross (weft) direction of the knitted mesh. Meshes were gamma sterilized at 25 kGy. Prior to cell seeding, meshes were rehydrated in PBS, transferred to culture medium overnight at 4°C, and rinsed with medium. Meshes were manually seeded using a pipette at a seeding density of 100,000 cells/cm^2 (250,000 cells/mesh) in 100 μL of medium per mesh and cultured for 24–48 h. The cells were seeded on top of the stabilized gelatin coating of the PA mesh, which was regularly checked for cell adherence. At the time of implantation, a confluent layer of cells was observed on the mesh surface (Fig. 1B). Control meshes of PA+G, without cells were incubated in culture medium only (Fig. 1A).

Implantation of eMSC-seeded mesh constructs

The experimental procedures and rat husbandry were approved by the Monash Medical Centre Animal Ethics Committee A (2011/61). CBH-rnu/Arc rats were housed in the animal house of Monash Animal Service facilities in compliance with the National Health and Medical Research Council guidelines for the care and use of laboratory animals. The rats were kept in closed cages with continuous automated air flow. The rats were provided with sterile food and water *ad libitum* and were kept under controlled environmental conditions at 20°C and a 12-h day/night cycle.

Seventy-four CBH-rnu/Arc immunodeficient nude rats were randomly divided into two experimental groups (37 rats/group) and were implanted with PA+G meshes, either with or without (controls) eMSC. The rats were anesthetized with 2.5% w/v Isoflurane® and analgesia was provided with Carprofen® (5 mg/kg bodyweight). The dorsum was disinfected with 0.5% Chlorhexidine® in 70% v/v ethanol and covered with sterile drapes. A longitudinal 30 mm skin incision was performed along the spine in the middle of the dorsum. Subcutaneous pockets were achieved by blunt dissection to both sides. Each mesh construct was subcutaneously implanted into each pocket. For each animal two meshes were inserted, one with the longitudinal axis cut in the machine direction of the knitted mesh, and the other cut in the cross direction. This was done to analyze the mechanical properties of both directions, since warp-knitted mesh is anisotropic. The animal ethics committee preferred the insertion of two smaller pieces of mesh on each side of the animal rather than one large piece of mesh across the dorsum. Each animal received either eMSC seeded or unseeded meshes. Meshes were secured in place using Vicryl 3-0® sutures on both ends. Skin closure was performed with a single intracutaneous Vicryl 3-0 suture. Following recovery, the animals were monitored daily until they were sacrificed at 7, 30, 60, and 90 days ($n=8$/group/timepoint) and 14 days ($n=5$) to track DiO-labeled cells on an additional time point. Each rat was euthanized in a CO_2 chamber. The animals were immediately inspected for signs of infection or seroma. Explanted meshes were dissected with a 0.5-cm border of adjacent tissue including skin and underlying muscles and divided into four parts, for biomechanical analysis, histology, immunohistochemistry, and flow cytometry, using the same pattern of dissection for each mesh.

Additionally, eMSC/PA+G construct dimensions were measured using electronic callipers and mesh contraction

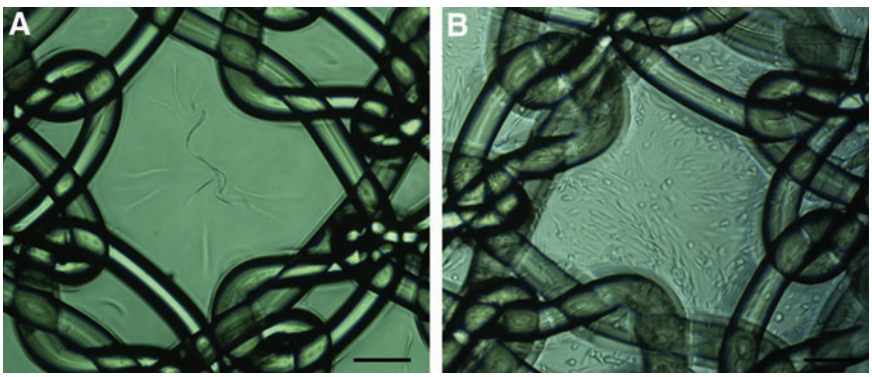

FIG. 1. PA+G mesh seeded **(A)** without and **(B)** with 100,000 cells/cm^2 48 h after cell seeding/noncell seeding, just prior to implantation. PA+G, polyamide mesh with gelatin coating. Scale bar indicates 200 μm. Color images available online at www.liebertpub.com/tea

calculated by dividing mesh area after explantation by the original mesh area. Explanted mesh pieces for biomechanical analysis were frozen at −20°C for subsequent testing.

Flow cytometry

A portion of the mesh with the surrounding tissue was collected for flow cytometry at 7, 14, 30, 60, and 90 days. A single cell suspension was obtained after fine mincing and filtering through a 10-μm cell strainer. Similarly, a 5×5×5-mm piece of brain, heart, lung, liver, and kidney were harvested, finely chopped, and filtered through the cell strainer. DiO-prelabeled cells were analyzed as described above. Rats without eMSC were used as the negative control.

Histology

For histological analysis, the explanted tissue from days 7, 30, 60, and 90 was fixed in 4% w/v paraformaldehyde (PFA) for 24 h, then embedded in paraffin and sectioned into 5 μm thick sections. After dewaxing and rehydrating in graded alcohols, sections were stained with hematoxylin and eosin (H&E) or Sirius Red F3B (0.1 g/100 mL saturated picric acid solution) (Sigma-Aldrich) for 1 h at room temperature (RT) to determine total collagen content, as described previously.[23] For the morphometric analysis, the stained slides were washed in running water (nonacidified) to remove the yellow picric acid counterstain and the residual red color imparted by the Sirius Red was quantified by image analysis.[23]

Paraffin sections were stained with anti rat CD68 antibody (details in Table 2) to identify tissue macrophages, and lightly counterstained with hematoxylin as described above. Sections underwent dewaxing, rehydrating in graded alcohols followed by antigen retrieval using citric acid buffer (0.1 M, pH 6.0), and microwaving for 5 min on high power. After cooling to RT and three washes in PBS, endogenous peroxidase was quenched by 3% w/v H_2O_2 followed by a protein block step (Protein Block; Dako) for 30 min at RT. The primary antibody and isotype controls (mouse IgG1) were incubated overnight at 4°C, sections washed, and the secondary antibody applied for 30 min at RT, as detailed in Table 2. Color was developed with 3,3′-diaminobenzidine (DAB) (Life Technologies). The slides were mounted with DPX (Scharlab).

Immunofluorescence

Tissue samples snap frozen in OCT were used for immunofluorescence and stained with antibodies to CD45 to visualize leukocytes, CCR7 for pro-inflammatory M1 macrophages, CD163 anti-inflammatory M2 macrophages, and anti-rat and anti-human collagen type I (Table 2). PFA fixed tissue was used to stain with αSMA to label smooth muscle cells. Thawed frozen sections (5 μm) were fixed in ice-cold acetone for 10 min. Pretreatment was performed for human collagen I according to the manufacturer's protocol. For αSMA, tissue was fixed and processed as described above, followed by protein block (Dako) for 30 min at RT. After three washes in PBS, primary antibodies were incubated for 1 h at 37°C; isotype-matched antibodies were used as negative controls and applied at the same concentration. Alexa-Fluor-488 and Alexa-Fluor-568-conjugated secondary antibodies (Table 2) were incubated for 30 min at RT, respectively. Nuclei were stained

Table 2. Details of Antibodies Used for Immunohistochemistry

Primary antibody	*Clone*	*Concentration*	*Isotype*	*Supplier*	*Secondary antibody*	*Concentration*	*Supplier*
Alpha-smooth muscle actin	1A4	1:400	Mouse IgG2a	Dako	Alexa fluor 488-goat anti-mouse IgG	1:200	Life Technologies®
CD 45 leukocyte common antigen	OX-1	1:200	Mouse IgG1	BD Pharmingen	Alexa fluor 568-donkey anti-mouse IgG (H+L)	1:200	Life Technologies
CD 68	ED1	1:500	Mouse IgG1	AbD Serotec	EnVison+System-HRP Labeled Polymer (anti-mouse)	Ready to use	Dako
Rat Collagen I	AB755P	1:60	Polyclonal IgG	Millipore	Alexa fluor 488-Goat anti-rabbit IgG	1:500	Life Technologies
Human Collagen I	MAB3391 (5D8-G9)	1:20	Mouse IgG_1	Millipore	Alexa fluor 488-donkey anti-mouse IgG (H+L) Ab150109	1:500	Sapphire Biosciences
CCR7 M1 marker		1:100	Polyclonal IgG	Sapphire Bioscience Pty. Ltd	Alexa568-goat anti-rabbit IgG	1:100	Life Technologies
CD163 M2 marker	ED2	1:400	Mouse IgG1	AbD Serotec	Alexa fluor 488 goat anti-mouse IgG	1:400	Life Technologies

with Hoechst 33258. The slides were mounted with fluorescent mounting medium (Dako).

Histomorphometric analysis of explanted tissues

Four images were taken per section stained with Sirius Red or immunostained for CD68, CCR7, CD163, αSMA, and CD45 for each explant at each time point using a Leica® DMR Fluorescence Microscope at 20× magnification. Images were captured from the four most central mesh filaments to achieve consistency; areas at anchoring sutures were excluded. The images were analyzed using image analysis software Metamorph (Molecular Devices, LLC) to measure positive staining around mesh filaments in 50 μm increments, as described previously.[23] The positive signal area (pixels) for every image was recorded and divided by the total tissue area examined. Cell numbers were calculated as positive area divided by the size of one representative cell using the Metamorph software. Collagen alignment was assessed using birefringence microscopy on the Sirius Red-stained slides and scored according to the presence of predominantly thick or thin birefringent fibers (0 = predominantly thin fibers, 1 = predominantly thick fibers).[27]

Biochemical analysis of collagens I and III

Sodium dodecyl sulfate–polyacrylamide gel electrophoresis (SDS-PAGE) using delayed reduction[28] was used to determine collagen type III/I ratio. Frozen tissue explants were thawed to RT for 15 min, and 5×5 mm pieces adjacent to the meshes were digested for 4 h (0.25 mg/mL pepsin (Sigma-Aldrich) in 100 mM acetic acid, pH 2.5) at 4°C followed by brief homogenization with a IKA T10 basic Ultra-Turrax®. Samples were then allowed to further digest in the pepsin solution for 16 h. Samples were then centrifuged, 10 μL of each sample mixed with 40 μL NuPAGE® LDS sample buffer (Life Technologies), heated to 90°C for 1–2 min, and then loaded onto NuPAGE 4%–12% Bis-tris gels (Life Technologies) with MES running buffer (Life Technologies); 50 mM (2-[*N*-morpholino]ethanesulfonic acid), 50 mM Tris base, 1 mM EDTA, 0.1% SDS; pH 7.3. Samples were electrophoresed for 1 h at 130 V, the power was then turned off, and 5% v/v 2-mercaptoethanol (Sigma-Aldrich) was added to each well and allowed to stand for 1 h. Finally, electrophoresis was continued for 3 h at 130 V at 4°C. Gels were stained with Coomassie Blue R-250 solution, destained in 20% ethanol and 5% acetic acid. Images were taken using FujiFilm LAS-3000 software. The percentage of type III collagen in type I and III collagen mixtures was calculated from peak sizes using the formula: percentage type III collagen = Area α1(III)×1.12×100/[Area α1(III)×1.12] + Area α1[I],[29] where a calibration factor of 1.12 was used to correct for the color yield from equal weights of the two collagen types.[29]

Mechanical analysis of explanted mesh constructs

Frozen explants were thawed at 4°C overnight and tested within 24 h of defrosting. We used a standard method of freezing and thawing the tissue, as published previously for urogynecological applications, which does not alter the tissue tensile properties.[30] Samples, of dimensions 4×25 mm, were punched from the explanted mesh piece along the longitudinal axis of the explanted mesh and kept moist using PBS until testing. Uniaxial tensiometry was performed on day 7 and 90 explants, with and without cells, using an Instron® Tensile Tester (5567® Instron Corporation) with a 5-kN load cell. Samples were secured in pneumatic serrated jaws to a 14-mm gauge length and extended to break at an elongation rate of 30 mm/min. Samples of the same dimensions were also punched from the preimplanted PA + G mesh in the knit machine and cross directions. PA + G mesh was soaked in PBS for at least 12 h and tested wet using the same procedure. Average load–elongation curves were plotted from the data generated. Mesh stiffness (N/mm) is represented by the slope of the load–elongation curve, with a steeper gradient indicating a stiffer mesh.

Statistics

GraphPad Prism 5.03.0001 was used for statistical analysis. Results are reported as mean ± SEM for each experimental group ($n = 8$ meshes/group/time point). For the biomechanical study, separate analyses were reported for the machine and cross direction meshes ($n = 8$/group/time point/mesh direction).

Since the data were not normally distributed (D'Agostino and Pearson omnibus normality test), nonparametric analysis using Kruskal–Wallis ANOVA for pairwise comparisons was undertaken followed by Bonferroni correction for assessment of differences between time points for the various meshes. p-Values < 0.05 were considered statistically significant.

Results

All animals had a normal postoperative recovery; none developed mesh erosion or any other side effects or died in the course of the experiment. All meshes, with and without seeded eMSC, were well tolerated as rats gained weight at all time points. Mesh contraction was rare and did not significantly differ between the rats treated with eMSC and the controls (without eMSC) or between the different time points.

Properties of passage 6 eMSC

$W5C5^+$ sorted-cells from the two samples cultured to P6 were pooled and analyzed as a single cell suspension. Colony forming unit activity was 0.04% ± 0.02% ($n = 3$ replicates), compared with 3.60 ± 1.56 for P0 $W5C5^+$ sorted cells. The P6 sorted cells differentiated into adipocytes, chondrocytes, myocytes, and osteocytes (Supplementary Fig. S1A–D; Supplementary Data are available online at www.liebertpub.com/tea), similar but to a lesser degree than P0 sorted cells. The P6 $W5C5^+$ population comprised 14.7% of cells, CD140b 15%, CD146 8.4%, CD29 97%, CD44 95%, CD73 97%, CD105 97%, CD34 0%, and CD45 0%, respectively (Supplementary Fig. S1E).

eMSC survival and tracking after implantation on the PA + G mesh

The fate of DiO-labeled eMSC implanted on the PA + G mesh was examined by flow cytometry. Before implantation 95% of cells were DiO^+ (Fig. 2A). Seven days after implantation DiO-labeled cells were found on the mesh (Fig. 2B); at 14 days a low percentage of cells were still present (Fig. 2C), but no cells were detected on day 30, 60, or 90 (Fig. 2D–F).

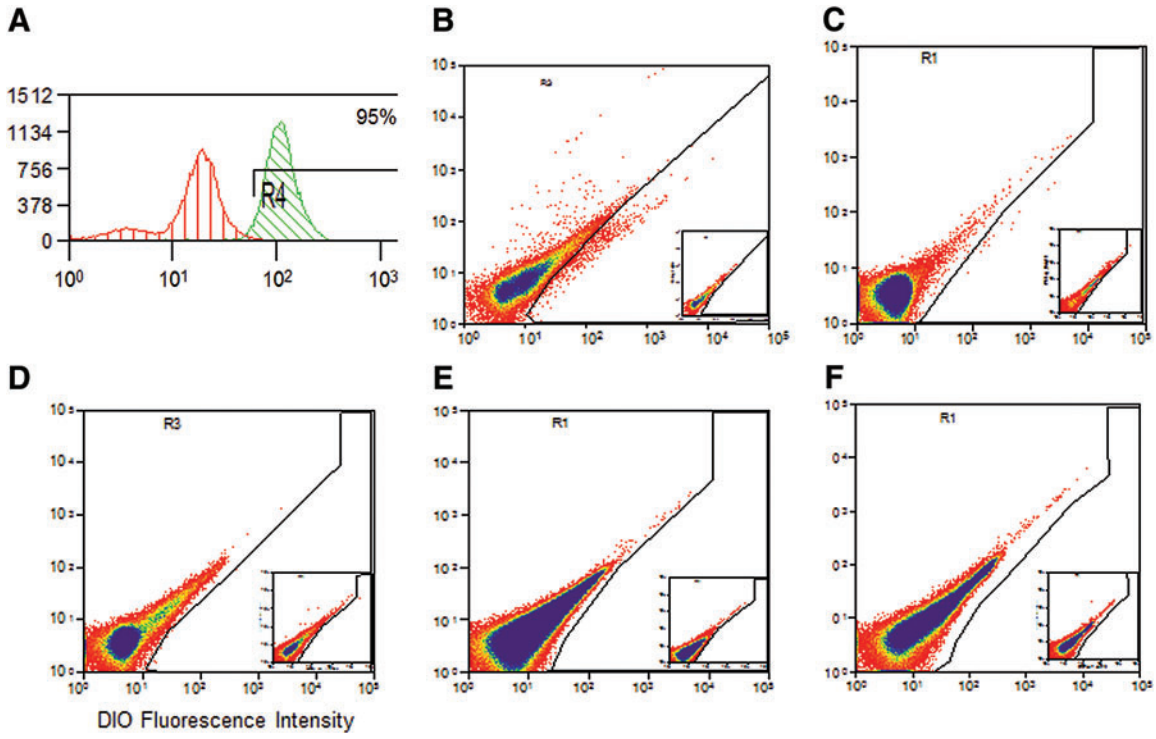

FIG. 2. Flow cytometric analysis of DiO-labeled cells. **(A)** Endometrial mesenchymal stem cells (eMSC) labeled with DiO prior to implantation. DiO^+ cells isolated from tissue explants at **(B)** 7 days, **(C)** 14 days, **(D)** 30 days, **(E)** 60 days, and **(F)** 90 days. Insets negative control (unlabeled cells). Representative plots from $n=6$ replicates showing DiO fluorescence intensity on the *x*-axis. Color images available online at www.liebertpub.com/tea

To determine whether eMSC had migrated from the implanted mesh constructs, the brain, lung, heart, liver, spleen, and kidney tissue at every time point was also analyzed by flow cytometry. No DiO^+ cells were observed in any of these organs at any time point.

Effect of eMSC on tissue response to the PA+G mesh

To examine the effect of implanted eMSC/PA+G constructs on histological changes we undertook a detailed analysis of the explanted TE constructs using histological stains, immunohistochemistry, and SDS gel electrophoresis. Representative images of H&E stained sections are shown in Supplementary Figure S2. As expected, at day 7 there was a vigorous cellular response between and around the mesh filaments in both cell-seeded and unseeded meshes (Supplementary Fig. S2A, B); in the cell-seeded meshes the response appeared more intense and may have been attributed to the presence of the seeded eMSC or a more apparent degradation of the gelatin in the presence of these cells. The degree of cellularity decreased with time but still persisted in both groups of meshes by day 90 (Supplementary Fig. S2C, D), although there was visually more new tissue formation within the implanted meshes in both groups. The connective tissue around the mesh filaments seems to be more organized in the meshes with eMSC on day 7 compared with the mesh alone. However, by day 90 there appeared less inflammatory cells around the filament bundles in the mesh with eMSC compared with the mesh alone. The gelatin was still present on day 7 in both groups as indicated by the arrows, whereas it was fully degraded by day 90.

Effect of eMSC on vascularization into the implanted PA+G mesh

To assess the extent of vascularization, we determined the profile area of αSMA immunostaining. At 7 days rats implanted with eMSC produced significantly more SMA positive vessel profiles compared with the controls ($p<0.05$) (Fig. 3A–C). There was no difference in the average content of smooth muscle cells for either eMSC treated or control rats at the later time points.

Effect of eMSC on inflammatory foreign body reaction to the PA+G mesh

The inflammatory response to the implanted TE constructs was evaluated by examining $CD45^+$ leukocyte density around mesh filaments (Fig. 4A, B) using image analysis.[23] CD45 leukocytes were concentrated both around the mesh perimeter and between the mesh filaments. The highest labeling index of the leukocyte infiltration was observed at 7 days with no significant differences between rats implanted with or without eMSC (Fig. 4C). At 30 and 60 days there was a decrease in both groups but no significant differences between the groups were observed. At 90 days, there were significantly fewer leukocytes surrounding the mesh filaments in rats treated with eMSC compared with controls ($p<0.05$) (Fig. 4A–C).

Since macrophages are the major leukocyte involved in the foreign body reaction,[23] we further quantified the level of $CD68^+$ cells. A similar pattern of labeling indices around the mesh filaments was observed for CD68 as for $CD45^+$ cells (Fig. 5). The highest macrophage accumulation was

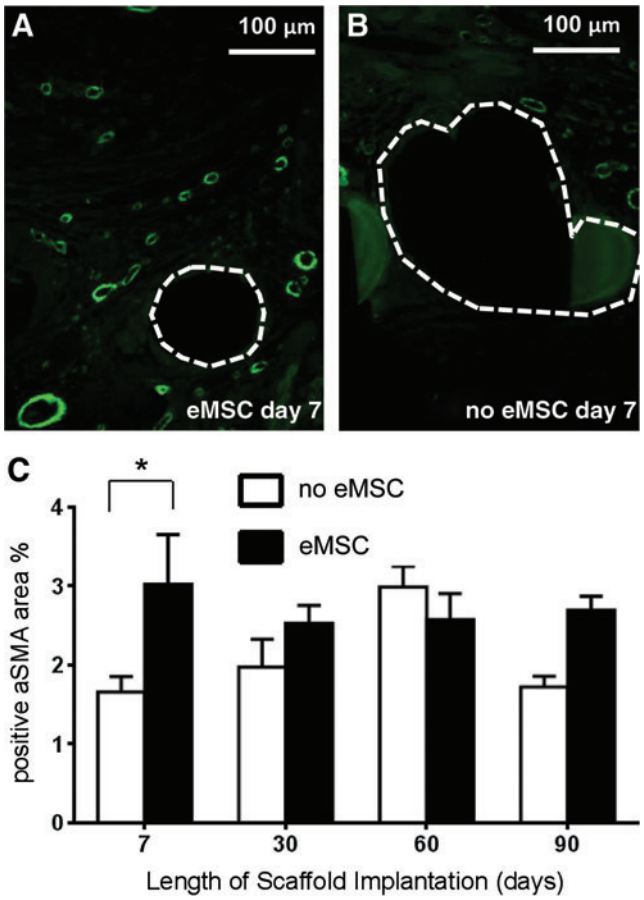

FIG. 3. Alpha-smooth muscle actin (αSMA) vessel immunostaining in explanted mesh constructs comprising PA+G meshes with (■) and without eMSC (□). At 7 days **(A)** with eMSC, **(B)** without eMSC. **(C)** αSMA positive area of vessel profiles (%), data are mean±SEM of $n=8$ animals/group, *$p<0.05$. Color images available online at www.liebertpub.com/tea

observed at 7 days, which significantly diminished by 90 days for both groups. Rats implanted with eMSC had significantly fewer macrophages at 90 days than rats without eMSC ($p<0.05$) (Fig. 5A–C). To determine whether the macrophages were pro-inflammatory or anti-inflammatory we stained the tissue with CCR7 and CD163 antibodies to detect M1 and M2 macrophages, respectively. The pro-inflammatory M1 cells were significantly higher in rats treated with eMSC at 7 days ($p<0.05$) with no significant differences at later time points (Fig. 5D). At 7 days, there was no difference in the level of M2 cells between the two groups. In the unseeded meshes, the total M1 plus M2 macrophage content was less than the CD68 levels, indicating that a significant proportion of infiltrating macrophages were uncommitted at this early stage. At 30 days M2 macrophages predominated in the eMSC-treated rats ($p<0.05$) (Fig. 5E). The number of anti-inflammatory M2 cells did not differ between groups at 7, 60, or 90 days. The M2/M1 ratio was significantly decreased at 7 days in the eMSC group ($p<0.001$), but no significant differences were observed at the later time points between the two groups (Fig. 5F).

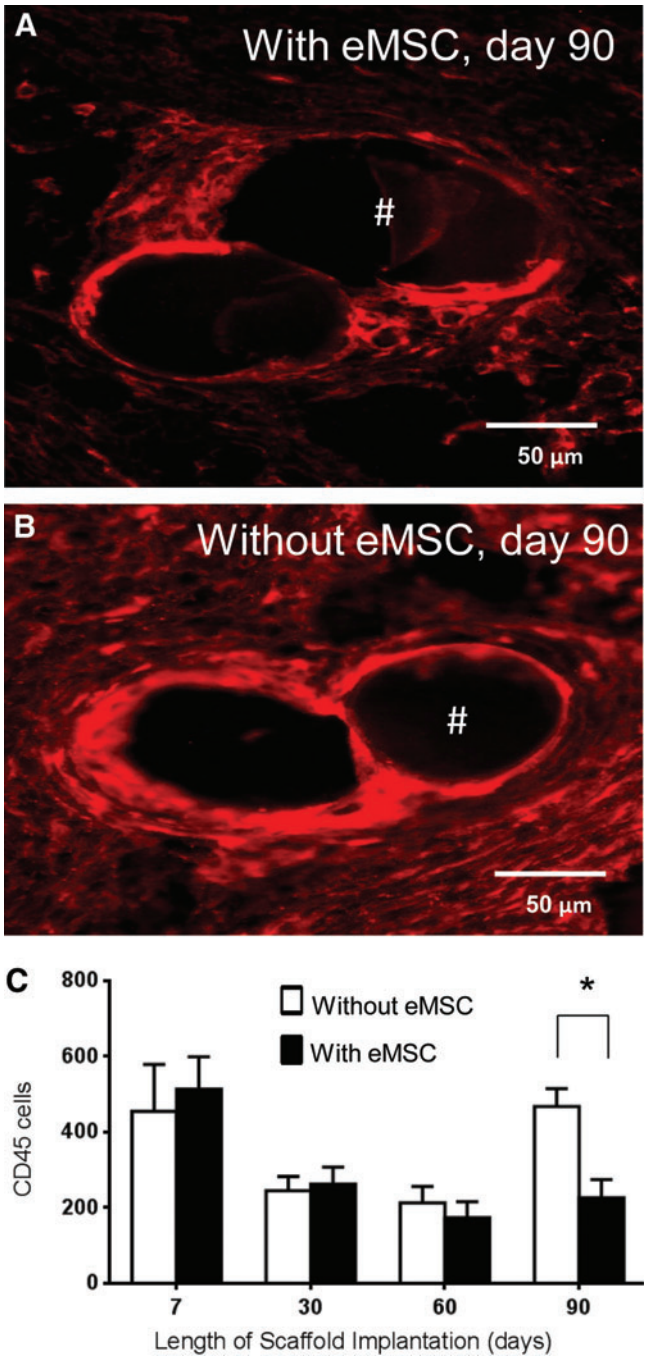

FIG. 4. CD45 immunostaining in explanted mesh constructs comprising PA+G meshes with and without eMSC. Day 90 explant **(A)** with eMSC, **(B)** without eMSC; Red staining indicates CD45 leukocytes. #, mesh filament. **(C)** Number of CD45-positive cells around mesh filaments from explants with (■) and without (□) eMSC. Data are mean±SEM of $n=8$ animals/group. *$p<0.05$. Color images available online at www.liebertpub.com/tea

Effect of eMSC on collagen deposition around the PA+G mesh

Sirius Red staining of total collagen deposition around mesh filaments (Fig. 6A, B) increased between day 7 and 60 in both eMSC treated and control meshes. Thereafter,

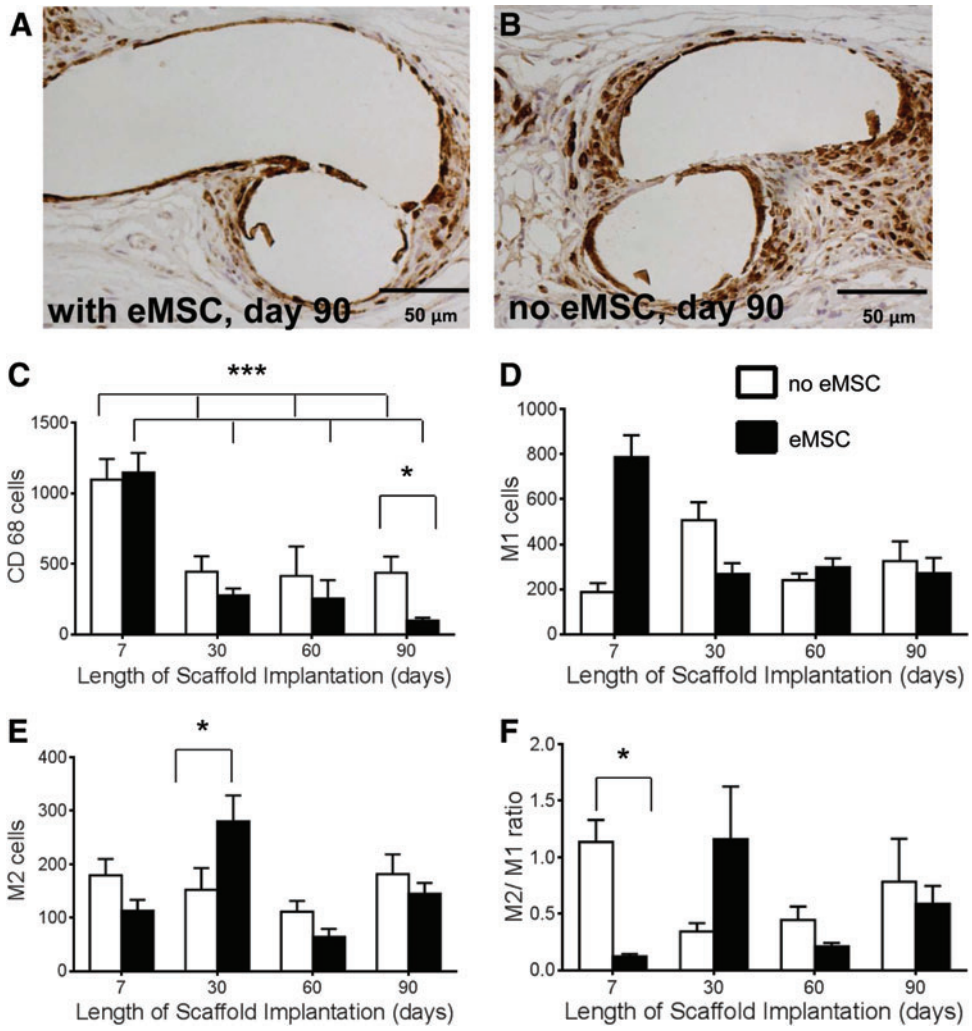

FIG. 5. Macrophage immunostaining in explanted mesh constructs comprising PA+G meshes with (■) and without (□) eMSC. Day 90 explant **(A)** with eMSC, **(B)** without eMSC. Positive cell numbers around mesh of **(C)** CD68 macrophages, **(D)** M1 macrophages (CCR7+), **(E)** M2 macrophages (CD263+), **(F)** M2/M1 ratio. Data are mean ± SEM of $n = 8$ animals/group. $^{*}p < 0.05$,$^{***}p < 0.001$. Color images available online at www.liebertpub.com/tea

the amount of collagen plateaued to 90 days (Fig. 6C). The percentage collagen type III within and around the meshes changed little with time in both meshes with and without cells, nor were there temporal differences (Fig. 6D). There were no significant differences in the percentage collagen type III in both seeded and unseeded meshes at any time point. Another important consideration is collagen organization. Our birefringence analysis showed that rats implanted with eMSC-seeded meshes had a greater number of thin collagen fibers, imaged with polarizing filters as green, after 90 days implantation, compared to meshes alone, where the fibers were thick and dense and yellow under polarized light (Fig. 6F, G). On day 90 explants, thin human fibers could be observed (Fig. 7B). The increased new collagen deposition seen at day 90 in Figure 7A was all rat collagen. Using antibodies that were specific to either rat or human collagen type I, cell-seeded 90 day explants showed uniform rat collagen type I within the PA fiber bundles (Fig. 7A) but no human collagen type I (Fig. 7B). Human endometrial tissue was used as a positive control for the anti-human collagen type I antibody (Fig. 7C) and the isotype control was always negative (Fig. 7D).

Effect of eMSC on the biomechanical properties of PA+G mesh

The average load–elongation curves for the day 7 and 90 explants, and the preimplanted PA+G mesh, in machine and the cross directions, are shown in Figure 8A–D. These load–elongation curves consisted of toe and linear regions, representing an initial region of low stiffness (toe region) followed by a region of higher stiffness (linear region), prior to failure (not shown). Explants without cells were stiffer (less extensible) than cell seeded explants, with increased stiffness in both toe and linear regions, at both time points and in both directions. For statistical analysis of load–elongation curves, 95% confidence intervals were plotted as error bars (Supplementary Fig. S3) to determine whether the differences were significant at the $p = 0.05$ level. Curves for day 7 and 90 explants originally seeded with cells were significantly different exceeding 2 mm elongation, in the cross (Supplementary Fig. S3A) and machine (Supplementary Fig. S3D) directions, respectively. Preimplanted PA+G meshes were generally of intermediate stiffness; between that of the explanted eMSC/PA+G and PA+G meshes. However, this result was only significant ($p < 0.05$) compared to the cell

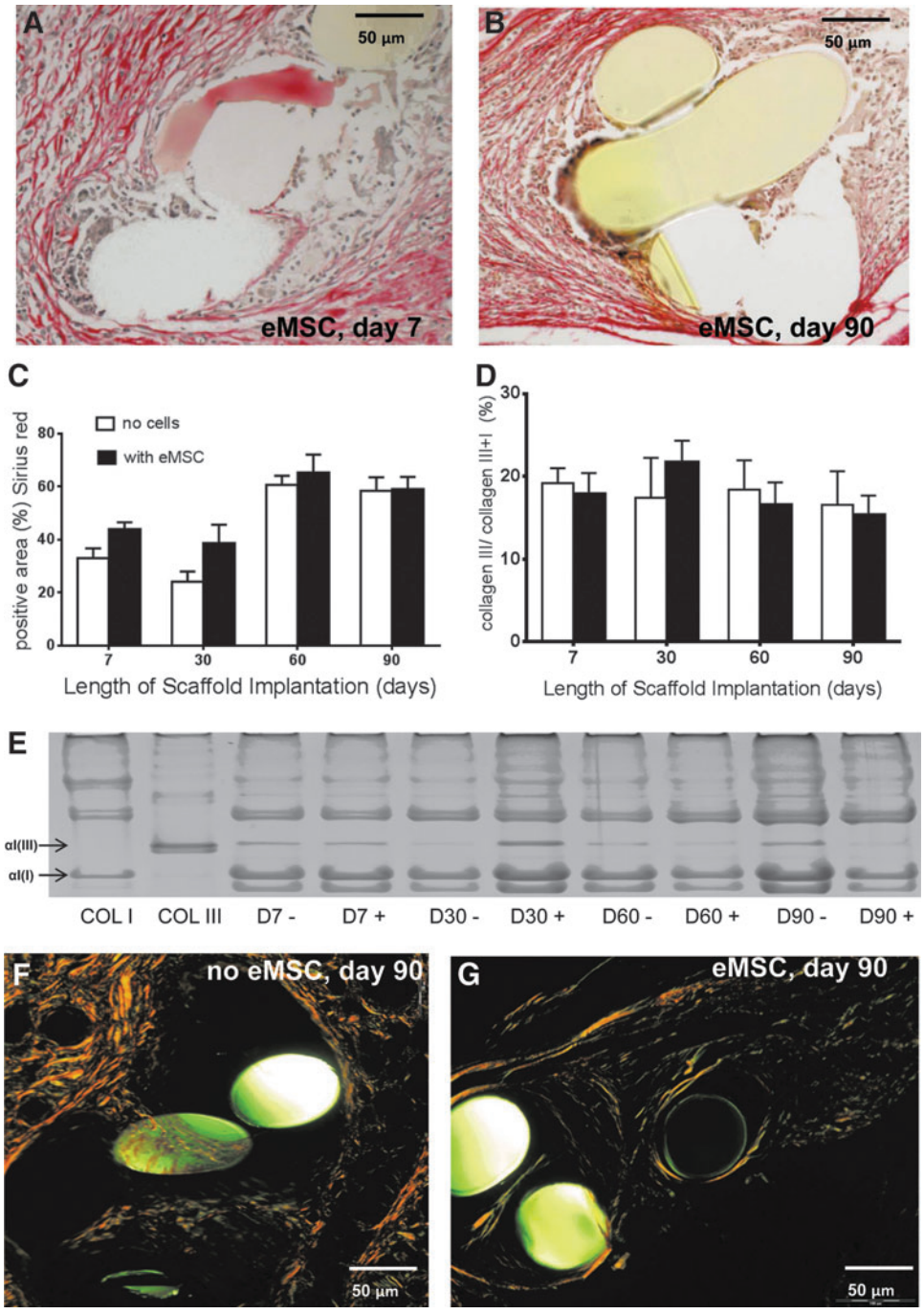

FIG. 6. Collagen quantification in explanted mesh constructs comprising PA+G meshes with (■) and without eMSC (□). Sirius Red staining of eMSC-seeded meshes at **(A)** 7 days, **(B)** 90 days. **(C)** Area of total collagen determined by Sirius Red staining **(D)** Percentage collagen type III determined by **(E)**. Sodium dodecyl sulfate–polyacrylamide gel electrophoresis (SDS-PAGE) gel analysis. Sirius Red birefringence at 90 days in explants **(F)** without eMSC and **(G)** with eMSC. Data are mean ± SEM of $n = 8$ animals/group.

seeded construct on day 7, in the cross direction (results not shown).

Discussion

The concept of delivering autologous differentiated cells or adult stem cells for POP repair has not been extensively validated, with only a few scattered reports[14,31–33] and no indications of ongoing or future clinical trials.[34,35] We previously showed that PA+G meshes induced a moderate foreign body reaction, neovascularization, and increased collagen deposition.[23] In this study, we have investigated the host inflammatory response, tissue integration, and mechanical properties of a novel mesh construct comprising PA+G, with and without seeded eMSC. The presence of seeded eMSC on the meshes was associated with clear quantitative differences in the type and extent of the tissue response, with controlled neotissue formation resulting in a more extensible and compatible integrated mesh. We showed that these eMSC delivered on novel PA+G meshes could be detected for up to 14 days after implantation, inducing higher initial neovascularization and acute inflammation, followed by a significantly reduced inflammatory response that was accompanied by a more organized collagen deposition. Seeded meshes were of decreased mechanical stiffness and higher extensibility compared with

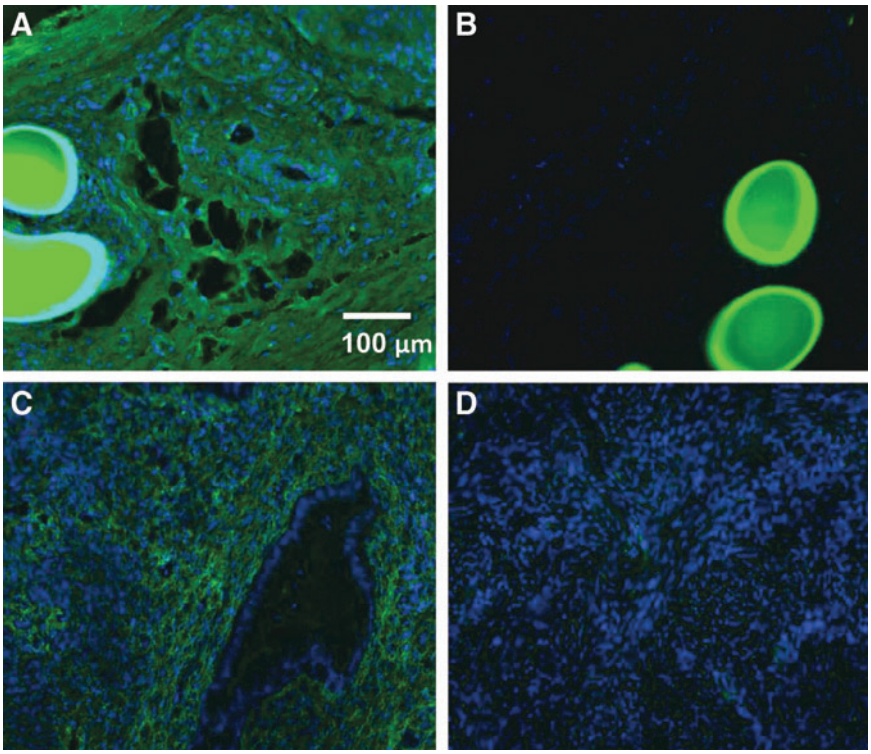

FIG. 7. Immunofluorescent detection of collagen type I in 90 day cell-seeded explants specifically stained for **(A)** rat collagen type I, and **(B)** human collagen type I; and in control human endometrial tissue stained for **(C)** human collagen type I or **(D)** isotype negative control.

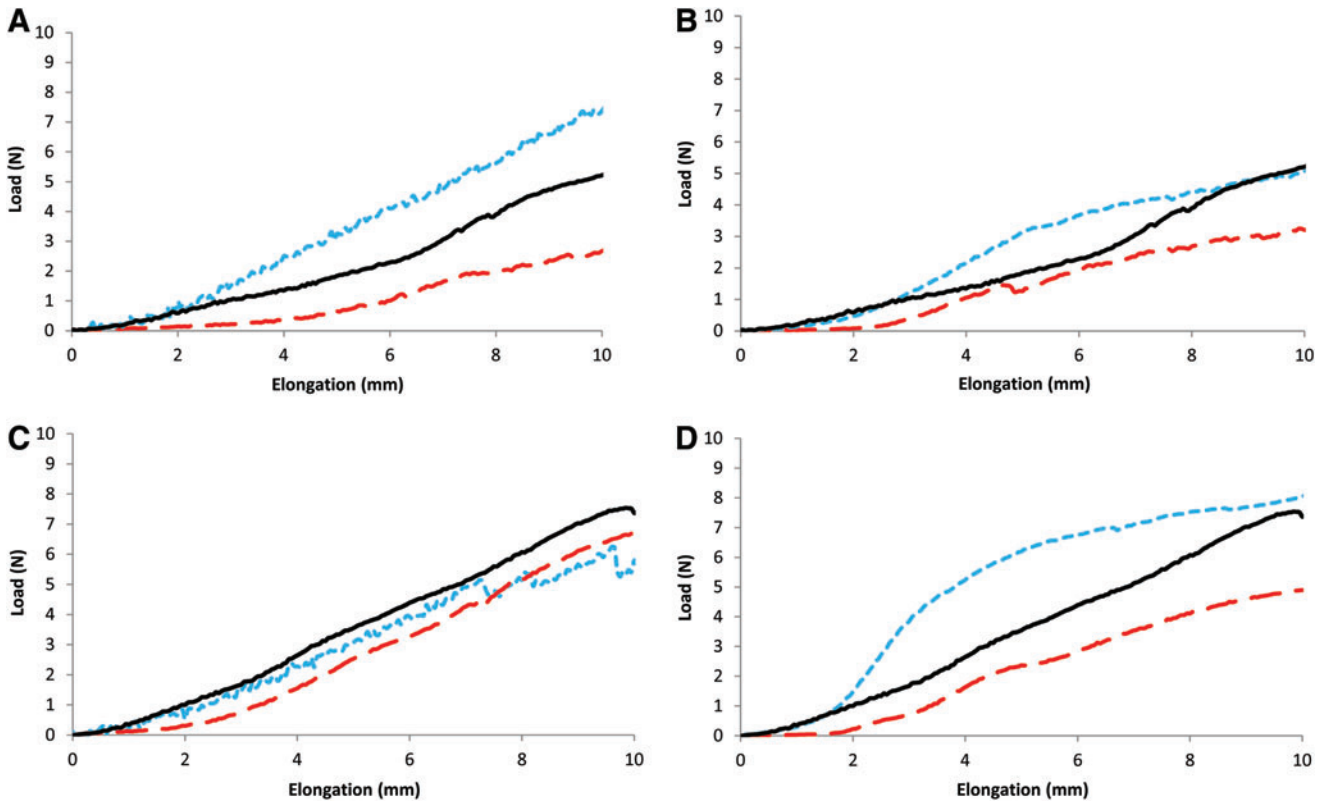

FIG. 8. Average load–elongation curves of explanted meshes ($n=8$) on **(A, C)** day 7 and **(B, D)** day 90 in mesh cross direction **(A, B)** and mesh machine direction **(C, D)**. Dashed line indicates meshes implanted with eMSC, dotted line indicates meshes implanted without eMSC, and solid line indicates preimplanted mesh ($n=6$). Color images available online at www.liebertpub.com/tea

unseeded mesh explants. Despite the lack of persistence of cells around the mesh filaments at the later time points, their initial modulatory effects appear to have influenced the nature of the chronic inflammatory response and mechanical tissue behavior in the long term. Meshes with eMSC had significantly reduced numbers of macrophages and leukocytes at 90 days suggesting that the eMSC may exert long-term anti-inflammatory effects. It is well known that bmMSC promote tissue repair via secreted soluble factors that recruit endogenous tissue stem cells to the site of injury,[36] and downregulating innate inflammatory and acquired immune responses, for example, by suppressing T lymphocytes, dendritic cells, and natural killer cells.[13,37] The exact immunomodulatory mechanism of MSC is still unclear; however, it has been shown that bmMSC can induce immunosuppression in the presence of IFN-γ and the concomitant presence of any of the three other proinflammatory cytokines, TNF-α, IL-1α, or IL-1β.[13] As the eMSC were not detected at 90 days it appears that these eMSC, like bmMSC, modulate the healing microenvironment through its paracrine or trophic effects, release signaling factors that reduce the inflammatory response even in the long term.[36] In our current study, it also appears that eMSC cytokines might influence the type of macrophage activity in the wound healing response as assessed by M1 and M2 phenotypic polarization.[38] Classically, the M1 macrophage phenotype and function is associated with pro-inflammatory responses, for example, activated by IFN-γ, microbial products, or antigens and can also lead to chronic inflammation, whereas the M2 phenotype encourages immunoregulation, tissue repair, and constructive tissue remodeling.[38,39] We observed that the meshes with eMSC had a significantly higher number of M1 macrophages at 7 days suggesting that in the nude xenograft animal model there is still substantial innate immunity with an influx of M1 macrophages either in response to the foreign human MSC or to the gelatin, which might more rapidly degrade in the presence of these cells. However, at 30 days a shift occurs and a significantly higher number of M2 macrophages were present in the rats implanted with eMSC suggesting that the eMSC may have promoted differentiation of the M1 to the M2 type macrophage. A recent study found that a high number of M2 macrophages at day 14 after intra-abdominal mesh implantation in a rat model was associated with preferable histological outcomes.[40] In our study, the M2/M1 ratio was highest in the seeded meshes at 30 days, but decreased at day 60 before again increasing at the later 90 day time point. This has been observed with biological cross-linked SIS implants where it was speculated that the transient relative increase in M1 or decrease in the M2/M1 ratio was due to degradation of the cross-links with time[39]; in our study, this may reflect the degradation peak of the gelatin substrate.

We also showed that neovascularization occurred more rapidly in the rats treated with eMSC as shown by the significantly higher number of αSMA-positive vessel profiles in the surrounding tissue at 7 days. In a recent study, a range of MSC populations from bone marrow, adipose, and dermal tissues were found to exert strong paracrine effects on neovascularization, promoting migration and proliferation of microvascular endothelial cells due to enhanced expression of the angiogenic factors, VEGF-A, bFGF, and others.[41] In our study, the level of vascularization remained constant over the course of implantation for the seeded meshes showing a trend to better vascularization even at 90 days compared with unseeded meshes. This early and sustained neovascularization induced by eMSC may promote neotissue formation from endogenous cells that accounts for the longer term improvement in tissue integration and mechanical properties of the newly formed tissue around the PA+G mesh.

Generally, the host wound healing response to implants occurs in various overlapping phases comprising inflammation, proliferation, tissue matrix formation, and remodeling.[31] Fibroplasia and collagen deposition begin in the proliferation zone and continues as the tissue becomes less cellular and remodels to a mature tissue or scar.[42] We found a slightly higher collagen content around the meshes in rats that had been seeded with eMSC although this was not statistically significant, suggesting that the eMSC might promote collagen production. The new collagen deposited within the mesh fibers over the course of implantation was of rat origin with no human collagen type I. This is consistent with our finding that the seeded human eMSC were only detected up to 14 days suggesting no trans-differentiation of these stem cells to collagen-producing human fibroblasts. It is more likely and consistent with the paracrine effects associated with these cells that the increased collagen results directly from the influx of surrounding rat fibroblasts. Collagen type I resides in most tissues, providing tensile strength and stiffness,[43,44] and collagen type III is abundant in extensible tissues.[44] Differences in fiber diameter, between types I and III, may account for differences in mechanical properties between them, with a reduction in collagen fiber diameter leading to a reduction in tensile strength.[45] In our study, collagen ratio did not significantly alter over time; however, there was a trend of decreasing collagen type III with time. This trend is in agreement with other studies that showed increased collagen type I/III over time in implants comprising PP, polyester, or a PP/polyglactin composite[46] and indicates normal physiological wound healing. What factors result in a normal physiological tissue is influenced not only by the collagen levels and types of collagens, but also by the quality of collagen and how it is remodeled.[47] Increased quantities of thin collagen fibers on eMSC seeded meshes on day 90, as determined by birefringence analysis, may have contributed to differences in observed biomechanical properties of the explants. The lower stiffness levels of the eMSC/PA+G meshes at all time points may have been due to these thinner, more deformable collagen fibers. However, as no difference in the collagen ratio was determined between eMSC/PA+G and PA+G meshes, differences in collagen fiber thickness may have been due to collagen packing and alignment.[48] In terms of collagen analysis not only is the amount of collagen important, but also the orientation or alignment of the collagen.[47] Both the unseeded and seeded meshes contained significant proportions of well aligned and packed collagen fiber bundles necessary for effective tensile strength within the new tissue. But, unlike the unseeded meshes where thicker fibers dominated, there was a good mix of thick orange fibers and a significant increase in green thinner fibers in meshes with cells at 90 days, indicative of a gradual remodeling that occurs in healthy new tissue formation as opposed to the continual expression of only overly thick fibers often

associated with scarring.[27] Scarless healing is important in the long term as scar tissue has less favorable mechanical properties than healthy tissue.[49] The endometrium is shed every month and heals without scarring[50] suggesting that eMSC could have a similar effect when transplanted in a xenogeneic model. It should be noted that our mechanical differences are related to the physiological stiffness of the new tissue formed; while we have not directly reported on the ultimate tensile strength, it is highly unlikely that this would have changed between the two mesh types (data not shown). It has recently been reported in POP repair that mesh stiffness is a primary clinical concern in the deterioration in biomechanical properties of the vagina;[51] so, our results on the role of eMSC on controlling tissue stiffness could impact on prevention of a common clinical sequelae.

The fate of implanted MSC after implantation is not yet clear, however, long-term engraftment seems to be rare.[52] We did not find eMSC in any of the organs, which is reassuring for future clinical applications. Similar to previous studies implanting MSC from other sources we found DiO-positive eMSC in the rats up to 14 days, but not in the long term.[53] Despite this they exert long-term effects that promote the biocompatibility of foreign bodies like synthetic mesh. It is unclear whether the cells die or rapidly proliferate leading to a dilution of the dye. However, we found that DiO-labeled eMSC retain the dye for up to 35 days *in vitro* (unpublished observation). In other studies, using DAPI-labeled muscle-derived stem cells onto SIS scaffolds[14] or DiI-labeled vaginal fibroblasts onto PLGA scaffolds,[32] visualization was found up to 4 and 12 weeks, respectively. The cell labeling itself needs to be validated; PKH126 and CFDA-SE labeling can reduce cell metabolic activity,[54] while there is a degree of variability in the use of the lypophilic membrane dyes.

A strength of this study was the use of image analysis software, which allows objective assessment of the cellular content, vascular tissue, and collagen.[23] However, the software was not able to detect differences in the collagen alignment, which was manually scored by using Sirius Red birefringence.

A limitation of this study is the choice of model for assessing *in vivo* biocompatibility of mesh to be used for endopelvic fascial defect repair as it does not mimic the vaginal milieu. However, we chose a skin wound repair model representative of vaginal skin repair using dorsal surface of the rat as proof of principle. The critical need for preclinical animal validation of new meshes and, in our current study, for cell-seeded meshes in POP repair, has been recently emphasized in the light of the high incidence of clinical implant failures.[55] However, this model can be used as a simulation of vaginal skin repair. We chose the rat dorsal wound model to exclude any effects due to loads or pressure as in the abdominal hernia model,[23,56] and therefore the effects observed would be due to the eMSC alone. In our previous evaluation of the new PA+G meshes in immunocompetent rats, we reported significant differences in the tissue response compared with the conventional PP meshes.[21] The rat is considered an ideal nonfunctional screening model for preclinical experiments to test the performance of new POP meshes.[57] The next step will be to test this TE construct in a large functional animal model of vaginal repair.[58]

Current treatment options for POP are either unsatisfactory when native tissue repair is used or are accompanied by high rates of adverse side effects when PP meshes are used for augmenting surgical reconstruction. A new treatment approach seems to be necessary. MSC have been shown to have great potential for soft tissue reconstruction[59] and if applied to vaginal surgery these cells might improve the long-term outcome by releasing factors that lead to a repair of the prolapsed tissue and improve biocompatibility by decreasing the foreign body reaction to implanted supporting meshes.

Our study reports that these new PA+G meshes seeded with eMSC are well tolerated, promote tissue integration, and reduce inflammatory reactions toward the implanted mesh in the longer term and may be a possible future treatment option for POP.

Acknowledgments

The authors acknowledge grant support from the Australian National Health and Medical Research Council grant 1021126 (C.E.G., J.A.W., A.R.) and Senior Research Fellowship 1042298 (C.E.G.), the CASS Foundation, South East Melbourne Alliance for Regenerative Therapies (C.E.G., J.A.W., A.R., S.L.E.), and the Victorian Government's Operational Infrastructure Support Program.

Disclosure Statement

No competing financial interests exist.

References

1. Haylen, B.T., de Ridder, D., Freeman, R.M., Swift, S.E., Berghmans, B., Lee, J., *et al.* An International Urogynecological Association (IUGA)/International Continence Society (ICS) Joint Report on the Terminology for Female Pelvic Floor Dysfunction. Neurourol Urodyn **29,** 4, 2010.
2. Hunskaar, S., Burgio, K., Clark, A., Lapitan, M.C., Nelson, R., Sillen, U., *et al.* Epidemiology of urinary (UI) and faecal (FI) incontinence and pelvic organ prolapse (POP). Available at: www.icsoffice.org/Publications/ICI_3/v1.pdf/chap5.pdf2005. Last accessed August 18, 2013.
3. Nygaard, I., Barber, M.D., Burgio, K.L., Kenton, K., Meikle, S., Schaffer, J., *et al.* Prevalence of symptomatic pelvic floor disorders in US women. Jama **300,** 1311, 2008.
4. Stanford, E.J., Cassidenti, A., and Moen, M.D. Traditional native tissue versus mesh-augmented pelvic organ prolapse repairs: providing an accurate interpretation of current literature. Int Urogynecol J **23,** 19, 2012.
5. Maher, C., Feiner, B., Baessler, K., Adams, E.J., Hagen, S., and Glazener, C.M. Surgical management of pelvic organ prolapse in women. Cochrane Database Syst Rev **4,** CD004014, 2010.
6. Konstantinovic, M.L., Pille, E., Malinowska, M., Verbeken, E., De Ridder, D., and Deprest, J. Tensile strength and host response towards different polypropylene implant materials used for augmentation of fascial repair in a rat model. Int Urogynecol J Pelvic Floor Dysfunct **18,** 619, 2007.
7. Delancey, J.O.L. Anatomic aspects of vagianl eversion after hysterectomy. Am J Obstet Gynecol **166,** 1717, 1992.
8. FDA Public Health Notification: Serious Complications Associated with Transvaginal Placement of Surgical Mesh in Repair of Pelvic Organ Prolapse and Stress Urinary Incontinence. 2008. Available at www.fda.gov/MedicalDevices/

Safety/AlertsandNotices/PublicHealthNotifications/UCM061976.htm. Last accessed August 18, 2013.
9. FDA Safety Communication: UPDATE on Serious Complications Associated with Transvaginal Placement of Surgical Mesh for Pelvic Organ Prolapse. 2011. Available at: www.fda.gov/MedicalDevices/Safety/AlertsandNotices/UCM262435.htm. Last accessed August 18, 2013.
10. Deprest, J., Zheng, F., Konstantinovic, M., Spelzini, F., Claerhout, F., Steensma, A., *et al.* The biology behind fascial defects and the use of implants in pelvic organ prolapse repair. Int Urogynecol J Pelvic Floor Dysfunct **17(Suppl 1),** S16, 2006.
11. de Tayrac, R., Alves, A., and Therin, M. Collagen-coated vs noncoated low-weight polypropylene meshes in a sheep model for vaginal surgery. A pilot study. Int Urogynecol J Pelvic Floor Dysfunct **18,** 513, 2007.
12. Lim, Y.N., Muller, R., Corstiaans, A., Hitchins, S., Barry, C., and Rane, A. A long-term review of posterior colporrhaphy with Vypro 2 mesh. Int Urogynecol J Pelvic Floor Dysfunct **18,** 1053, 2007.
13. Shi, Y., Hu, G., Su, J., Li, W., Chen, Q., Shou, P., *et al.* Mesenchymal stem cells: a new strategy for immunosuppression and tissue repair. Cell Res **20,** 510, 2010.
14. Ho, M.H., Heydarkhan, S., Vernet, D., Kovanecz, I., Ferrini, M.G., Bhatia, N.N., *et al.* Stimulating vaginal repair in rats through skeletal muscle-derived stem cells seeded on small intestinal submucosal scaffolds. Obstet Gynecol **114,** 300, 2009.
15. Deprest, J., De Ridder, D., Roovers, J.P., Werbrouck, E., Coremans, G., and Claerhout, F. Medium term outcome of laparoscopic sacrocolpopexy with xenografts compared to synthetic grafts. J Urol **182,** 2362, 2009.
16. Dolce, C.J., Stefanidis, D., Keller, J.E., Walters, K.C., Newcomb, W.L., Heath, J.J., *et al.* Pushing the envelope in biomaterial research: initial results of prosthetic coating with stem cells in a rat model. Surg Endosc **24,** 2687, 2010.
17. Gargett, C.E., Nguyen, H.P.T., and Ye, L. Endometrial regeneration and endometrial stem/progenitor cells. Rev Endocr Metab Disord **13,** 235, 2012.
18. Gargett, C.E., Schwab, K.E., Zillwood, R.M., Nguyen, H.P., and Wu, D. Isolation and culture of epithelial progenitors and mesenchymal stem cells from human endometrium. Biol Reprod **80,** 1136, 2009.
19. Gargett, C.E., Chan, R.W.S., and Schwab, K.E. Endometrial stem cells. Curr Opin Obstet Gynecol **19,** 377, 2007.
20. Masuda, H., Anwar, S.S., Buehring, H-J., Rao, J.R., and Gargett, C.E. A novel marker of human endometrial mesenchymal stem-like cells. Cell Transplant **21,** 2201, 2012.
21. Rajaraman, G., White, J., Tan, K.S., Ulrich, D., Rosamilia, A., Werkmeister, J.A., *et al.* Optimisation and scale up culture of human endometrial multipotent mesenchymal stromal cells: potential for clinical application. Tissue Eng Part C Methods **19,** 80, 2013.
22. Edwards, S.L., Werkmeister, J.A., Rosamilia, A., Ramshaw, J.A.M., White, J.F., and Gargett, C.E. Characterisation of clinical and newly fabricated meshes for pelvic organ prolapse repair. J Mech Behav Biomed Mater **23,** 53, 2013.
23. Ulrich, D., Edwards, S.L., White, J.F., Supit, T., Ramshaw, J.A.M., Lo, C., *et al.* A preclinical evaluation of alternative synthetic biomaterials for fascial defect repair using a rat abdominal hernia model. PLoS One **7,** 2012.
24. Schwab, K.E., and Gargett, C.E. Co-expression of two perivascular cell markers isolates mesenchymal stem-like cells from human endometrium. Hum Reprod **22,** 2903, 2007.
25. Buhring, H.J., Battula, V.L., Treml, S., Schewe, B., Kanz, L., and Vogel, W. Novel markers for the prospective isolation of human MSC. Ann N Y Acad Sci **1106,** 262, 2007.
26. Dominici, M., Le Blanc, K., Mueller, I., Slaper-Cortenbach, I., Marini, F., Krause, D., *et al.* Minimal criteria for defining multipotent mesenchymal stromal cells. The International Society for Cellular Therapy position statement. Cytotherapy **8,** 315, 2006.
27. Junqueira, L.C.U., Bignolas, G., and Brentani, R.R. Picrosirius staining plus polarization microscopy, a specific method for collagen detection in tissue-sections. Histochem J **11,** 447, 1979.
28. Sykes, B., Puddle, B., Francis, M., and Smith, R. Estimation of 2 collagens from human dermis by interrupted gel-electrophoresis. Biochemical and Biophys Res Commun **72,** 1472, 1976.
29. Chan, D., and Cole WG. Quantitation of type I and type-III collagens using electrophoresis of alpha chains and cyanogen-bromide peptides. Anal Biochem **139,** 322, 1984.
30. Rubod, C., Boukerrou, M., Brieu, M., Dubois, P., and Cosson, M. Biomechanical properties of vaginal tissue. Part 1: new experimental protocol. J Urol **178,** 320, 2007.
31. De Philippo, R.E., Bishop, C.E., Freitas, L., Yoo, J.J., and Atala, A. Tissue engineering a complete vaginal replacement from a small biopsy of autologous tissue. Transplantation **86,** 208, 2008.
32. Hung, M.J., Wen, M.C., Hung, C.N., Ho, E.S.C., Chen, G.D., and Yang, V.C. Tissue-engineered fascia from vaginal fibroblasts for patients needing reconstructive pelvic surgery. Int Urogynecol J **21,** 1085, 2010.
33. de Filippo, R.E., Yoo, J.J., and Atala, A. Engineering of vaginal tissue *in vivo*. Tissue Eng **9,** 301, 2003.
34. Martin, I., Baldomero, H., Bocelli-Tyndall, C., Passweg, J., Saris, D., and Tyndall, A. The Survey on Cellular and Engineered Tissue Therapies in Europe in 2010. Tissue Eng Part A **18,** 2268, 2012.
35. Ulrich, D., Muralitharan, R., and Gargett, C. Toward the use of endometrial and menstrual blood mesenchymal stem cells for cell-based therapies. Expert Opin Biol Ther **13,** 1387, 2013.
36. Caplan, A.I., and Dennis, J.E. Mesenchymal stem cells as trophic mediators. J Cell Biochem **98,** 1076, 2006.
37. Di Nicola, M., Carlo-Stella, C., Magni, M., Milanesi, M., Longoni, P.D., Matteucci, P., *et al.* Human bone marrow stromal cells suppress T-lymphocyte proliferation induced by cellular or nonspecific mitogenic stimuli. Blood **99,** 3838, 2002.
38. Mantovani, A., Sica, A., and Locati, M. Macrophage polarization comes of age. Immunity **23,** 344, 2005.
39. Badylak, S.F., Valentin, J.E., Ravindra, A.K., McCabe, G.P., and Stewart-Akers, A.M. Macrophage phenotype as a determinant of biologic scaffold remodeling. Tissue Eng Part A **14,** 1835, 2008.
40. Brown, B.N., Londono, R., Tottey, S., Zhang, L., Kukla, K.A., Wolf, M.T., *et al.* Macrophage phenotype as a predictor of constructive remodeling following the implantation of biologically derived surgical mesh materials. Acta Biomater **8,** 978, 2012.
41. Hsiao, S.T.-F., Asgari, A., Lokmic, Z., Sinclair, R., Dusting, G.J., Lim, S.Y., *et al.* Comparative analysis of paracrine factor expression in human adult mesenchymal stem cells derived from bone marrow, adipose, and dermal tissue. Stem Cells Dev **21,** 2189, 2012.

42. Midwood, K.S., Williams, L.V., and Schwarzbauer, J.E. Tissue repair and the dynamics of the extracellular matrix. Int J Biochem Cell Biol **36,** 1031, 2004.
43. Prockop, D.J., and Kivirikko, K.I. Collagens-molecular-biology, diseases, and potentials for therapy. Annu Rev Biochem **64,** 403, 1995.
44. Gelse, K., Poschl, E., and Aigner, T. Collagens—structure, function, and biosynthesis. Adv Drug Deliv Rev **55,** 1531, 2003.
45. Doillon, C.J., Dunn, M.G., Bender, E., and Silver, F.H. Collagen fiber formation in repair tissue-development of strength and toughness. Coll Relat Res **5,** 481, 1985.
46. Junge, K., Klinge, U., Klosterhalfen, B., Mertens, P.R., Rosch, R., Schachtrupp, A., *et al.* Influence of mesh materials on collagen deposition in a rat model. J Invest Surg **15,** 319, 2002.
47. Feola, A., Abramowitch, S., Jones, K., Stein, S., and Moalli, P. Parity negatively impacts vaginal mechanical properties and collagen structure in rhesus macaques. Am J Obstet Gynecol **203,** 2010.
48. Dayan, D., Hiss, Y., Hirshberg, A., Bubis, J.J., and Wolman, M. Are the polarization colors of Picrosirius Red-stained collagen determined only by the diameter of the fibres. Histochemistry **93,** 27, 1989.
49. Jean-Charles, C., Rubod, C., Brieu, M., Boukerrou, M., Fasel, J., and Cosson, M. Biomechanical properties of prolapsed or non-prolapsed vaginal tissue: impact on genital prolapse surgery. Int Urogynecol J **21,** 1535, 2010.
50. Salamonsen, L.A. Tissue injury and repair in the female human reproductive tract. Reproduction **125,** 301, 2003.
51. Feola, A., Abramowitch, S., Jallah, Z., Stein, S., Barone, W., Palcsey, S., *et al.* Deterioration in biomechanical properties of the vagina following implantation of a high-stiffness prolapse mesh. BJOG **120,** 224, 2013.
52. von Bahr, L., Batsis, I., Moll, G., Hagg, M., Szakos, A., Sundberg, B., *et al.* Analysis of tissues following mesenchymal stromal cell therapy in humans indicates limited long-term engraftment and no ectopic tissue formation. Stem Cells **30,** 1575, 2012.
53. Zimmermann, C.E., Gierloff, M., Hedderich, J., Acil, Y., Wiltfang, J., and Terheyden, H. Survival of transplanted rat bone marrow-derived osteogenic stem cells *in vivo*. Tissue Eng Part A **17,** 1147, 2011.
54. Polzer, H., Volkmer, E., Saller, M.M., Prall, W.C., Haasters, F., Drosse, I., *et al.* Long-term detection of fluorescently labeled human mesenchymal stem cell *in vitro* and *in vivo* by semi-automated microscopy. Tissue Eng Part C Methods **18,** 156, 2012.
55. Deprest, J., and Feola, A. The need for preclinical research on pelvic floor reconstruction. BJOG **120,** 141, 2013.
56. Konstantinovic, M.L., Lagae, P., Zheng, F., Verbeken, E.K., De Ridder, D., and Deprest, J.A. Comparison of host response to polypropylene and non-cross-linked porcine small intestine serosal-derived collagen implants in a rat model. BJOG **112,** 1554, 2005.
57. Abramowitch, S.D., Feola, A., Jallah, Z., and Moalli, P.A. Tissue mechanics, animal models, and pelvic organ prolapse: A review. Eur J Obstet Gynecol Reprod Biol **144,** S146, 2009.
58. Frey-Vasconcells, J., Whittlesey, K.J., Baum, E., and Feigal, E.G. Translation of stem cell research: points to consider in designing preclinical animal studies. Stem Cells Transl Med **1,** 353, 2012.
59. Atala, A. Tissue engineering of reproductive tissues and organs. Fertil Steril **98,** 21, 2012.

Address correspondence to:
Caroline E. Gargett, PhD
Monash Institute of Medical Research
27-31 Wright Street
Clayton, VIC 3168
Australia

E-mail: caroline.gargett@monash.edu

Received: March 15, 2013
Accepted: September 25, 2013
Online Publication Date: November 11, 2013